true beam shape) with the UGC and IRAS samples we find that $I(<z_{max})/\langle I\rangle \approx (30\pm15)\%$ ($f/0.5$). It encompasses the estimate of ~20% made by Piccinotti *et al.* (ref. 17) on the basis of source counts of bright AGNs. We therefore conclude that the X-ray foreground could be due to AGNs. Modest evolution of AGN can then account for the X-ray background, provided that there is some (not yet fully understood) spectral evolution (for example, ref. 21) because the background has a power-law spectrum with energy index of 0.4, whereas most AGNs at low z have an energy index[22] of ~0.7. It is possible that there is another class of source contributing, but it must have a lower local emissivity than AGNs.

Our strong cross-correlation signal is not in conflict with the stringent limits on the auto correlation signals[13,23,24]. For a euclidean universe, the auto-correlation of the X-ray flux which originates from sources in a shell (R_{min}, R_{max}) in a square beam at 'zero-lag' is

$$W_{xx} \approx (a^2\langle n\rangle R_{min}R_{max}^2)^{-1} + A_\gamma a^{1-\gamma}/(2-\gamma)(r_0/R_{max})^\gamma. \quad (6)$$

This illustrates that auto-correlation is a strongly decreasing function of R_{max} and that it is expected to be much weaker than W_{xg} as it originates from $R_{max} \gg R_{eff}$, (that is, the signal is smeared out along the line of sight). Indeed, the analysis of the auto-correlation of the Ginga scans[13] has shown that an AGN population could produce the entire XRB between redshift 0.05 and 3, if their correlation length is smaller than $9h^{-1}$ Mpc, without exceeding observed limits on the auto-correlation.

In conclusion, the cross-correlation signal indicates that a non-negligible fraction of the XRB background can be produced by unevolved X-ray sources correlated with optical and IRAS galaxies. However, this is not sufficient to explain the entire XRB and its spectrum, without invoking evolution of the sources, or a new population at high redshift. □

Received 15 February; accepted 29 June 1993.

1. Turner, E. L. & Geller, M. J. *Astrophys. J.* **236,** 1–5 (1980).
2. Jahoda, K., Lahav, O., Mushotzky, R. F. & Boldt, E. A. *Astrophys. J.* **378,** L37–L40 (1991); erratum in *Astrophys. J.* **399,** L107 (1992).
3. Wu, X., Hamilton, T., Helfand, D. J. & Wang, Q. *Astrophys. J.* **379,** 564–575 (1990).
4. Hasinger, G., Schmidt, M. & Trümper, J. *Astr. Astrophys.* **246,** L2–L5 (1991).
5. Shanks, T. *et al. Nature* **353,** 315–320 (1991).
6. Fabian, A. C. & Barcons, X. *A. Rev. Astr. Astrophys.* **30,** 429–456 (1992).
7. Peebles, P. J. E. *The Large Scale Structure of the Universe* (Princeton Univ. Press, 1980).
8. Lahav, O. in *The X-Ray Background* (eds Barcons, X. & Fabian, A. C.) 102–107 (Cambridge Univ. Press, 1992).
9. Lahav, O., Nemiroff, R. J. & Piran, T. *Astrophys. J.* **350,** 119–124 (1990).
10. Saunders, W., Rowan-Robinson, M. & Lawrence, A. *Mon. Not. R. astr. Soc.* **258,** 134–146 (1992).
11. Nilson, P. *Uppsala General Catalogue of Galaxies, Uppsala Astr. Obs. Ann.* Vol. 6 (1973).
12. Meurs, E. J. A. & Harmon, R. T. *Astr. Astrophys.* **206,** 53–62 (1989).
13. Carrera, F. J. *et al. Mon. Not. R. astr. Soc.* **260,** 376–384 (1993).
14. Yahil, A., Strauss, M. A., Davis, M. & Huchra, J. P. *Astrophys. J.* **372,** 380–393 (1991).
15. Strauss, M. A. *et al. Astrophys. J. Suppl. Ser.* **83,** 29–63 (1992).
16. Boldt, E. in *The X-Ray Background,* (eds Barcons, X. & Fabian, A. C.) 115–137 (Cambridge Univ. Press, 1992).
17. Piccinotti, G. *et al. Astrophys. J.* **253,** 485–503 (1982).
18. Awaki, H. thesis, Univ. Nagoya (1991).
19. Griffiths, R. E. & Padovani, P. *Astrophys. J.* **360,** 483–489 (1990).
20. Boldt, E. *Phys. Reports* **146,** 215–257 (1987).
21. Schwartz, D. A. & Tucker, W. H. *Astrophys. J.* **332,** 157–162 (1988).
22. Turner, T. J. & Pounds, K. A. *Mon. Not. R. astr. Soc.* **240,** 833–880 (1989).
23. De Zotti, G. *et al. Astrophys. J.* **351,** 22–30 (1990).
24. Jahoda, K. & Mushotzky, R. F. in *The X-Ray Background* (eds Barcons, X. & Fabian, A. C.) 80–96 (Cambridge Univ. Press, 1992).

Ejection of dust from Jupiter's gossamer ring

Douglas P. Hamilton & Joseph A. Burns*

Astronomy Department, and * Theoretical and Applied Mechanics Department, Cornell University, Ithaca, New York 14853, USA

One of the most intriguing discoveries of the Ulysses mission so far has been the detection of periodic, collimated streams of high-velocity, submicrometre-sized dust particles emanating from Jupiter[1,2]. To explain the Ulysses data, Horanyi *et al.* showed[3] that electromagnetic forces within Jupiter's magnetosphere can accelerate and eject small dust particles; they proposed a model in which Io is the source of the dust, and the observed periodicity arises from a resonance between the orbital and rotational periods of Io and Jupiter respectively. Here we argue that the masses and velocities of the detected particles are better explained by an origin in Jupiter's gossamer ring. Following their ejection from the magnetosphere, the dust particles are accelerated by the interplanetary magnetic field (IMF). We find that it is the temporal evolution of the IMF which primarily determines the particle trajectories, and hence which particles reach the spacecraft. Our model explains three main features observed in the Ulysses data: fewer streams are detected before closest approach than after, the observed periodicity is closely related to the solar rotation period, and an extremely intense dust stream is detected immediately after closest approach.

We describe first how dust may be ejected from the vicinity of Jupiter (compare ref. 3). When viewed in a non-rotating, jovian-centred reference frame, a charged particle is subject to the so-called co-rotational electric field which arises from Jupiter's spinning magnetic field[4,5]. The potential associated with this electric field can be readily incorporated into an orbital energy equation if we confine our analysis to nearly equatorial orbits, consider only the dominant aligned dipolar component of the jovian magnetic field, and assume that the electric charge of a grain remains constant[6,7]. Because the kinetic energy of escaped particles equals the total energy (kinetic + potential) of grains on initially circular orbits, such particles will be ejected at speed

$$v_\infty = \left(\frac{2GM_J}{R}\left(L-\frac{1}{2}\right)\right)^{1/2} \quad (1)$$

where G ($=6.67\times10^{-8}$ cm^3 s^{-2} g^{-1}) is the gravitational constant, M_J ($=1.9\times10^{30}$ g) is the jovian mass, R is the initial distance of the particle from Jupiter, and L is the ratio of the Lorentz force arising from the electric field to Jupiter's gravity[5]. Near Jupiter

$$L \sim 0.0057\left(\frac{1\ \mu m}{r_g}\right)^2\left(\frac{\Phi_g}{1\ V}\right)\left(\frac{1\ g\ cm^{-3}}{\rho_g}\right) \quad (2)$$

where Φ_g, r_g, and ρ_g are the surface potential, radius, and mass density of the grain respectively[5]. The charge on circumplanetary grains is determined by a balance between electron, ion, photoelectric, and secondary electron emission currents; in the jovian ring, the latter three currents may be strong enough to induce positive charges. Following refs 3 and 8, we choose $\Phi_g = +3$ V and $\rho = 1$ g cm^{-3} as an illustrative example.

Since v_∞ in equation (1) must be real, only particles with $L > 1/2$ (which are small and positively-charged) can escape; taking our assumptions for charge and density, $L \gtrsim 1/2$ implies $r_g < r_g^{max} \sim 0.18$ μm, or $m_g \lesssim 2.6\times10^{-14}$ g. Particles larger than r_g^{max} are gravitationally dominated and bound to Jupiter; moreover, because L is independent of R, r_g^{max} will not vary with the source location. The tiniest particles have large charge-to-mass ratios and hence spiral (gyrate) tightly around magnetic field lines like electrons and ions do; accordingly these particles are also bound to Jupiter. Particles of intermediate size experience weaker electromagnetic forces and hence have larger gyroradii. Only when gravity is relatively weak and gyroradii are large (for grain radii satisfying $r_g^{min} < r_g < r_g^{max}$) do the orbital dynamics

accelerate positively charged particles away from Jupiter (in Table 1 we list r_g^{min} as determined numerically).

Potential sources of dust in Jupiter's magnetosphere include the main ring[9] (1.7–1.8 R_J), the gossamer ring[10] (1.8–3.0 R_J), and Io[11] (5.9 R_J); dust is thought to be generated in the rings by impacts on parent bodies that slowly abrade away[12], whereas dust that is lofted in Io's volcanic plumes can be swept into the jovian magnetosphere[3,11]. We now test these sites for their escape characteristics under the assumption that dust begins on initially circular, uninclined keplerian orbits. First, by considering the Jacobi constant, which is conserved in the rotating frame, one can show that particles launched from circular orbits within synchronous orbit ($R_{syn} = 2.24\ R_J$) are unable to escape regardless of their charge histories[13]; thus the main jovian ring can be ruled out as the source of any particles detected by Ulysses.

Table 1 lists the escape characteristics of dust from Io and from two locations in the gossamer ring. Particles from the gossamer ring, especially the denser portion between synchronous orbit and the moon Amalthea (2.5 R_J), are found to escape with maximum speeds similar to those observed by Ulysses[2] (60 km s^{-1}). Furthermore, the masses of these escaping particles cover the observed two orders of magnitude[2]. By contrast, if volcanos on Io supply the dust streams, then some escaping particles could have speeds of ~300 km s^{-1}, well in excess of those observed by Ulysses, but still within the sensitivity range of its dust detector[14,15]. In addition, the mass ratio for Io particles is ~8,000, nearly 100 times the measured mass ratio. These results are all robust in that they are independent of the magnitude of the assumed grain charge as long as it remains nearly constant. For Io to be a viable source, an additional mechanism must be invoked to prevent escape of the smallest grains.

TABLE 1 Properties of particles escaping from Jupiter

Source region	$R(R_J)$	L_{crit}	r_g^{min} (μm)	m_g^{max}/m_g^{min}	v_∞ (km s^{-1})
Near synchronous orbit	2.25	4.4	(0.062)	26	<77
Outer gossamer ring	3.0	22	(0.028)	290	<150
Io	5.9	200	(0.009)	8,000	<340

Possible source regions and their distances from Jupiter in jovian radii (R_J ~ 71,500 km) are shown, followed by L_{crit}, the numerically-determined force ratio for the smallest escaping grains. The size of these smallest grains (r_g^{min}) is determined from equation (2) using $L = L_{crit}$, $\rho_g = 1$ g cm^{-3}, and $\Phi_g = +3$ V. The mass ratio m_g^{max}/m_g^{min} is found by solving equation (2) for r_g^3, using first $L = 1/2$ (which corresponds to the largest escaping grain regardless of source) and then $L = L_{crit}$. The final column lists numerically determined escape speeds which agree well (to within a few per cent) with those found from equation (1). With the exception of the minimum grain size, all quantities in this table are independent of the assumed grain charge and density.

Particles leave the jovian system along nearly equatorial trajectories because sources are in the equatorial plane and the primary acceleration is radial. Nevertheless, numerical integrations show that the ~10° tilt in the jovian magnetic field causes typical trajectories to bend 10 to 20° out of the plane. These inclinations may allow escaping grains to avoid the densest parts of the Io torus (where grains charge negatively, possibly preventing their escape[8]) by flying above or below it. Later, the distorted field of the middle magnetosphere will augment the bending, but

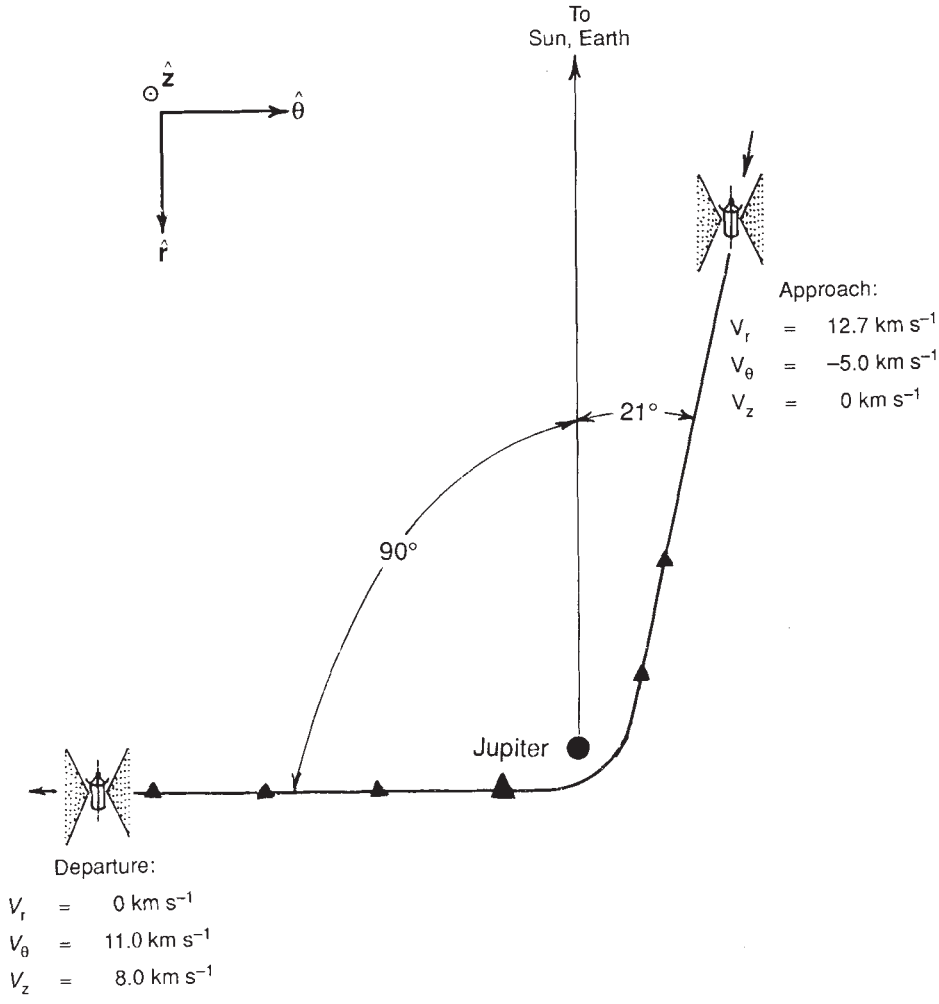

FIG. 1 The trajectory of the Ulysses spacecraft as seen from Jupiter and projected into the Earth's orbital plane (the ecliptic) which is tilted only a few degrees with respect to Jupiter's equatorial plane. The directions $\hat{\mathbf{r}}$, $\hat{\boldsymbol{\theta}}$ and $\hat{\mathbf{z}}$ point radially outward, roughly along Jupiter's velocity vector, and toward the ecliptic north respectively. Ulysses, represented by the butterfly-shaped icon, spins around an axis which is directed toward Earth; the shaded triangular wings suggest the spin-averaged directional sensitivity of the dust detector. The components of the spacecraft's velocity relative to Jupiter are listed before and after encounter and, to a good approximation, are valid during all of the stream events. Evenly spaced triangles along the Ulysses trajectory indicate the locations at which dust streams were detected; average stream duration and separation were one day and 28 ± 3 days, respectively[2]. During these events, characteristic particle velocities ranged from 20 to 60 km s^{-1} while masses varied from 10^{-16} to 10^{-14} g. The stream immediately after closest approach (large triangle) was particularly noteworthy, containing many more particles than all of the other streams combined[2].

not significantly for swift grains.

Once in interplanetary space, the motion of a typically-charged grain is dominated by Lorentz forces which greatly exceed solar gravity[2]. On average, the interplanetary magnetic field at Jupiter lies in the ecliptic, counterclockwise from (and within 10° of) the $\hat{\boldsymbol{\theta}}$ direction (Fig. 1)[16]. Thus, because the solar wind convects the magnetic field with velocity $v_{sw}\hat{\mathbf{r}}$, the induced electric field $\mathbf{E} = -v_{sw}\hat{\mathbf{r}} \times \mathbf{B}$, and hence the vertical acceleration, points primarily in the $\pm\hat{\mathbf{z}}$ direction (toward or away from the ecliptic plane). The magnitude of this acceleration varies because both the solar wind's velocity and especially its embedded **B** field change with a roughly 26–29-day periodicity imposed by solar rotation; stochastic variations further complicate this simple picture[17]. Nevertheless, throughout the interplanetary portion of the trajectory of a dust grain, vertical ($\hat{\mathbf{z}}$) accelerations overwhelm horizontal ones indicating that the ecliptic component of the grain's velocity remains essentially constant.

We now demonstrate how a periodic vertical acceleration may lead to episodic detections of dust. We represent the acceleration by successive intervals of constant strengths and consider both a symmetric profile (Fig. 2*a*) and an asymmetric one (Fig. 3*a*). Vertical displacements are found by integrating the acceleration twice; these solutions consist of linked parabolic segments (Figs 2*b* and 3*b*). In both cases, the exact three-dimensional distribution of all ejected dust particles is complicated, depending on the range of dust particle positions and velocities upon escape from the jovian magnetosphere, as well as the detailed history of the solar wind speed and magnetic field strength. Nevertheless, we can still draw some qualitative conclusions.

According to our interpretation, the periodicity of the Ulysses detections stems from the periodicity of the vertical acceleration which causes the paths of particles to intersect the spacecraft trajectory only at certain times. As time progresses in Figs 2*c* and 3*c*, each element of the dust distribution moves to the right along its own streamline at the ejection speed; thus a stationary point near streamline B will receive dust only once every solar cycle (~28 days). Stationary points near the ecliptic plane should experience subharmonic streams at roughly twice this rate (every 14 days). These periods will differ somewhat from those measured by Ulysses because Ulysses moves to a new position and a new streamline between detections. Owing to the directional sensitivity of the dust detector, the subharmonic streams predicted in the ecliptic could be weak; nevertheless, they should be sought when the Ulysses data is further processed.

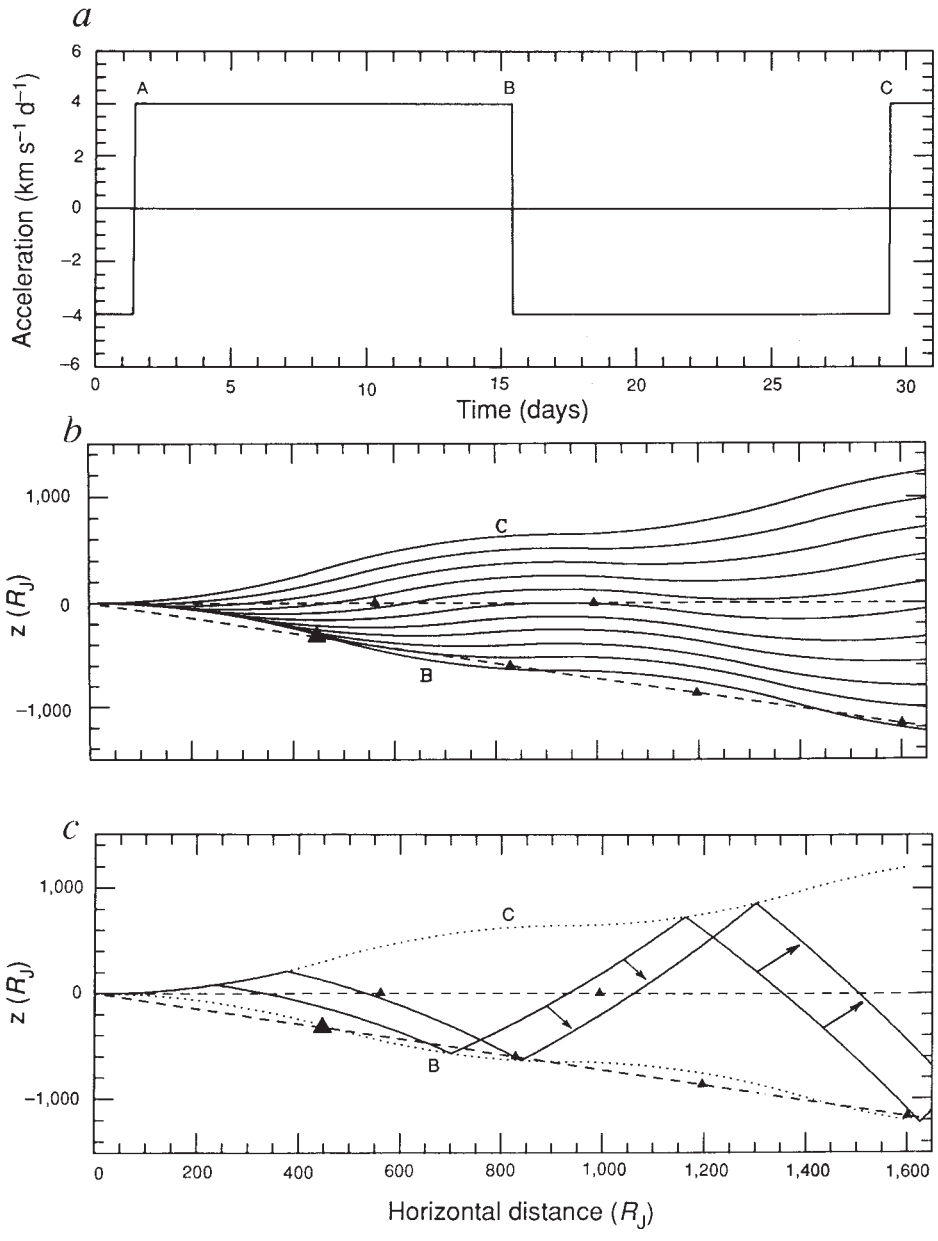

FIG. 2 Motion of charged dust grains relative to Jupiter. Grains are accelerated by a time-varying symmetric interplanetary magnetic field after being launched from Jupiter in the ecliptic plane with velocities of 40 km s^{-1}. *a*, The acceleration experienced by a charged grain is constant (4 km s^{-1} d^{-1}), but changes sign every 14 days (roughly half of a solar rotation period); its magnitude corresponds to a 0.1 μm grain and solar wind parameters of $B \sim 5$ nT and $v_{sw} \sim 600$ km s^{-1} (ref. 2). *b*, Streamlines for particles launched between times B and C in *a* (that is at various times when the initial acceleration is downward. The vertical ($\hat{\mathbf{z}}$) direction is defined in Fig. 1). Jupiter is at (0, 0), the horizontal dashed line is Ulysses' incoming trajectory and the diagonally descending dashed line represents its outgoing path. The solid triangles show the locations of the detected dust streams with the largest signifying the single intense burst. Note that the bottommost streamline corresponds to particles launched at time B in *a*, whereas the topmost is for those starting at time C; the undulations visible in each streamline are caused by changes in the sign of the acceleration. Particles launched between times A and B follow streamlines that are the mirror image of those shown here; in particular the dense concentration of streamlines is found above the ecliptic plane. *c*, Streamlines B and C (dotted) and the Ulysses path (dashed) are as in *b*. The solid lines oscillating back and forth through $z = 0$ are snapshots of a pair of dust distributions for grains continuously injected over 50 days. The two distributions are separated by about 4 days with the arrows indicating the motion in the intervening time.

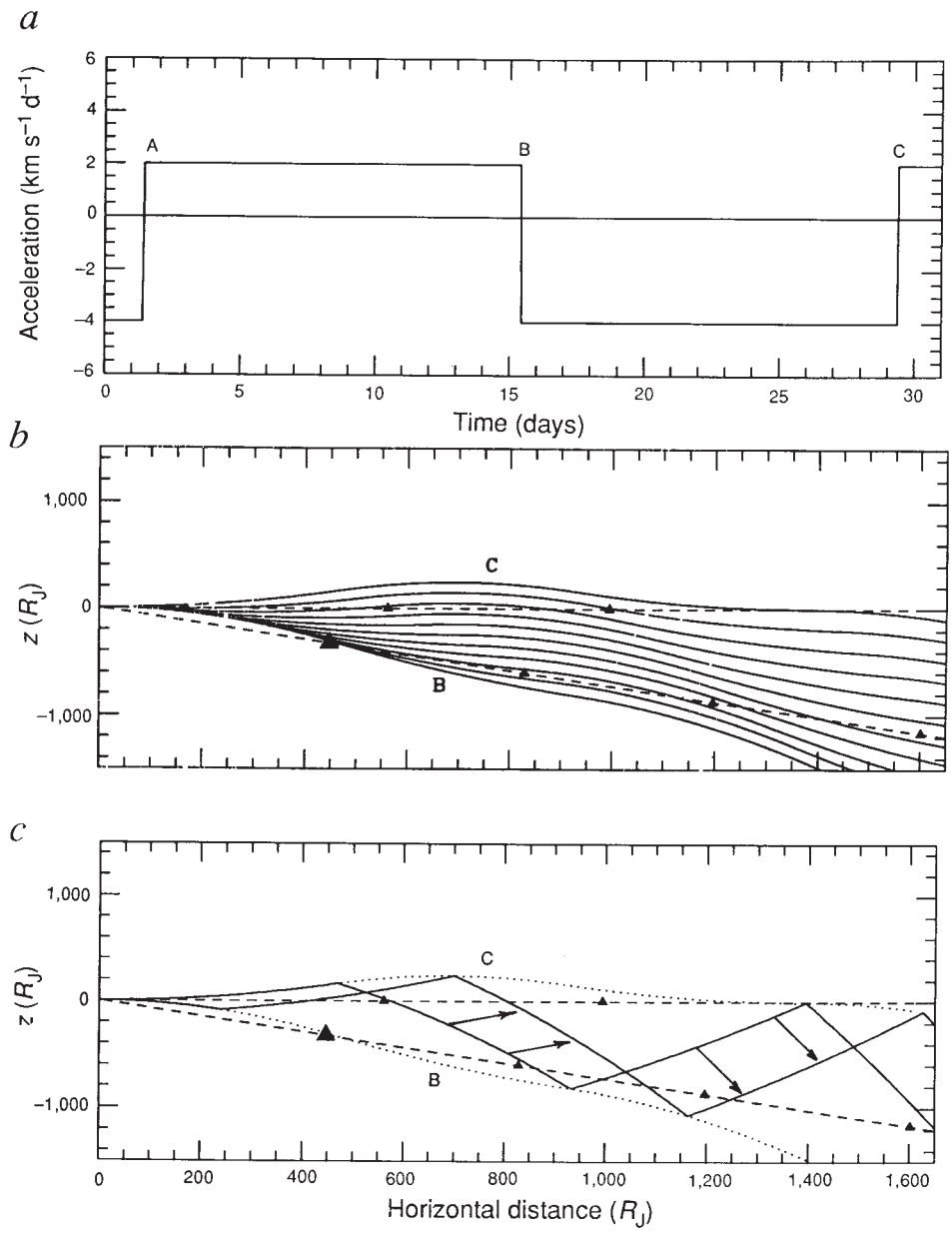

FIG. 3 Motion of a dust grain relative to Jupiter in an asymmetric model of the interplanetary magnetic field; symbols and axes are the same as the corresponding panels (*a*, *b*, *c*) of Fig. 2. *a*, The acceleration experienced by a charged grain in the time-varying asymmetric interplanetary magnetic field. *b*, Because of the asymmetry, the average acceleration felt by a grain over a long period is negative; hence streamlines are swept downward eventually leaving the ecliptic plane free of dust. *c*, The two dust distributions shown here are separated by 7 days; both occur at slightly later times than the distributions in Fig. 2*c*.

Differences in the number of streams detected in and out of the ecliptic plane can arise from asymmetry in the vertical acceleration (Fig. 3), which itself has many causes: corotating interaction regions, configuration of the solar current sheet, distribution of sunspots and coronal holes and so on[17,18]. Asymmetry imparts a non-zero vertical acceleration which sweeps particles away from the ecliptic plane. This may explain why only two dust streams were detected before closest approach (when the spacecraft was in the ecliptic plane), whereas four were sensed afterwards (with the spacecraft descending beneath the plane). The detection geometry, which was more favourable after closest approach than before, may also be important (Fig. 1).

Streamlines are clearly most concentrated at the lower left in Figs 2*b* and 3*b*; half a cycle later these enhancements are found at the upper left. Streamline clustering occurs because particles launched at different times will follow the same parabolic trajectory through space as long as the acceleration remains pointed in one direction. Furthermore, when $L \gg 1/2$ the ejection mechanism and the subsequent vertical acceleration are both wholly electromagnetic and even particles of different sizes will initially follow the identical path albeit with different speeds. These dense concentrations of streamlines never cross the ecliptic and disperse once the acceleration changes sign. Our model therefore predicts that intense streams should be detected only near Jupiter and only out of the ecliptic plane, in agreement with the timing and position of the single intense stream detected ~30 days after closest approach (Figs 2 and 3).

We conclude that solar modulations of the interplanetary magnetic field are primarily responsible for the periodicity, distribution, and relative intensities of stream events detected by the Ulysses spacecraft and that the gossamer ring is their most likely source. These results are not critically dependent on the magnitude of the assumed grain charge. □

Received 25 May; accepted 14 June 1993.

1. Grün, E. *et al. Science* **257,** 1550–1552 (1992).
2. Grün, E. *et al. Nature* **362,** 428–430 (1993).
3. Horanyi, M., Morfill, G. & Grün, E. *Nature* **363,** 144–146 (1993).
4. Burns, J. A. & Schaffer, L. E. *Nature* **337,** 340–343 (1989).
5. Hamilton, D. P. *Icarus* **101,** 244–264 (1993).
6. Schaffer, L. E. *thesis* Cornell Univ. (1989).
7. Horanyi, M. & Burns, J. A. *J. geophys. Res.* **96,** 19283–19289 (1991).
8. Horanyi, M., Morfill, G. & Grün, E. *J. geophys. Res.* (submitted).
9. Showalter, M. R., Burns, J. A., Cuzzi, J. N. & Pollack J. B. *Icarus* **69,** 458–498 (1987).
10. Showalter, M. R., Burns, J. A., Cuzzi, J. N. & Pollack J. B. *Nature* **316,** 526–528 (1985).

11. Johnson, T. V., Morfill, G. & Grün, E. *Geophys. Res. Lett.* **7,** 305–308 (1980).
12. Burns, J. A., Showalter, M. R. & Morfill, G. E. in *Planetary Rings* (eds Greenberg, R. & Brahic, A.) 200–272 (Univ. of Arizona, Tucson, 1984).
13. Schaffer, L. E. & Burns, J. A. *J. geophys. Res.* (submitted).
14. Grün, E. *et al. Space Sci. Rev.* **60,** 317–340 (1992).
15. Grün, E. *et al. Astr. Astrophys. Suppl. Ser.* **92,** 411–423 (1992).
16. Fisk, L. A. in *The Ancient Sun* (eds Pepin, R. O., Eddy, J. A. & Merill, R. B.) 103–118 (Pergamon, New York, 1980).
17. Smith, E. J. in *The Sun in Time* (eds Sonett, C. P., Giampapa, M. S. & Matthews, M. S.) 175–201 (Univ. of Arizona, Tucson, 1991).
18. Smith, E. J., Slavin, J. A. & Thomas, B. T. in *The Sun and the Heliosphere in Three Dimensions* (ed. Marsden, R. G.) 267–274 (Reidel, Dordrecht, 1986).

ACKNOWLEDGEMENTS. We thank M. Horanyi for discussion, E. Grün for sharing data, and V. Chang, I. Mosqueira and P. Nicholson for critically reading the manuscript, and C. Murray for comments.

Activation of a carbon–carbon bond in solution by transition-metal insertion

Michael Gozin, Alexander Weisman, Yehoshua Ben-David & David Milstein*

Department of Organic Chemistry, The Weizmann Institute of Science, Rehovot 76100, Israel

* To whom correspondence should be addressed

CLEAVAGE of carbon–carbon bonds by transition-metal-containing heterogeneous catalysts forms the basis of one of the most important industrial processes, the refining of petroleum to chemicals and fuels[1]. But the generally low product selectivity observed with heterogeneous systems is a significant drawback. For this reason, much effort has been devoted to developing transition-metal complexes that can be inserted into C–C bonds in homogeneous media, as such catalysts can operate under mild, easily controlled conditions and might offer high selectivity and reactivity. Metal insertion into C–H bonds is well known[2,3–5], but, except in a few special cases[2,6–12], C–C bonds are generally unreactive towards insertion of transition metals in solution. Here we report the selective activation of a simple C–C bond by a mononuclear rhodium complex in a neutral homogeneous medium (tetrahydrofuran solution). We are able to effect Rh insertion into a C–C bond in a diphosphinoxylene, in which this bond is favourably oriented towards the transition-metal centre. The competing reaction of insertion into C–H is suppressed by the use of an overpressure of H_2. We suggest that this approach might lead to a general strategy for C–C activation in homogeneous systems.

Carbon–carbon bonds are generally unreactive towards the insertion of soluble metal complexes, except when activated by strain[2,6], when there is a drive to aromatic character in pre-aromatic systems[7–10], or in the presence of a carbonyl group[11,12]. β-Alkyl transfer in highly Lewis-acidic complexes has been reported[13,14]. To investigate the possibility of transition-metal insertion into a C–C bond in solution, we planned to use a metal hydride complex, which (if capable of insertion into C–C) would eliminate methane and thereby render the process thermodynamically feasible. The expected competing reaction, the kinetically favourable insertion into C–H, would probably be reversible even if hydrogen is eliminated and might be pushed backwards under hydrogen (Fig. 1).

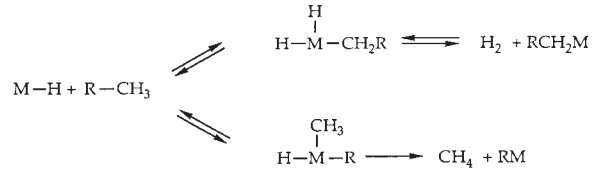

FIG. 1 Hypothesis for C–C activation under hydrogen. (R is an alkyl or aryl group.)

α,α'-Diphosphino-*m*-xylenes undergo C–H activation forming bis-chelated complexes[15–17]. Probing for the possibility of directed C–C cleavage, we prepared the new phosphine, shown as **1** in Fig. 2. Reaction of **1** with $HRh(P(C_6H_5)_3)_4$ in a tetrahydrofuran (THF) solution at 25 °C results in exclusive C–H activation to yield quantitatively the thermally stable Rh(I) complex **2**, with liberation of hydrogen. The pure complex was fully characterized by ^1H, ^{13}C and ^{31}P NMR and its structure was confirmed by a single-crystal X-ray structural study (Fig. 3), which shows that (1) the metal-bound Ar–C(7) bond (where Ar = aryl) is not weakened relative to the other Ar–C bonds in this molecule, (2) there is no distortion from aromaticity, the aromatic ring and the carbon atoms bound to it retaining planarity, (3) to maintain a favourable square-planar arrangement around the rhodium atom, a relatively weak $Rh–CH_2Ar$ bond is formed as reflected by the distorted C(1)–C(7)–Rh(I) angle of 92.8 (4)°.

Remarkably, heating of **2** at 90 °C under hydrogen at a pressure of 80 p.s.i. results in quantitative C–C cleavage, yielding

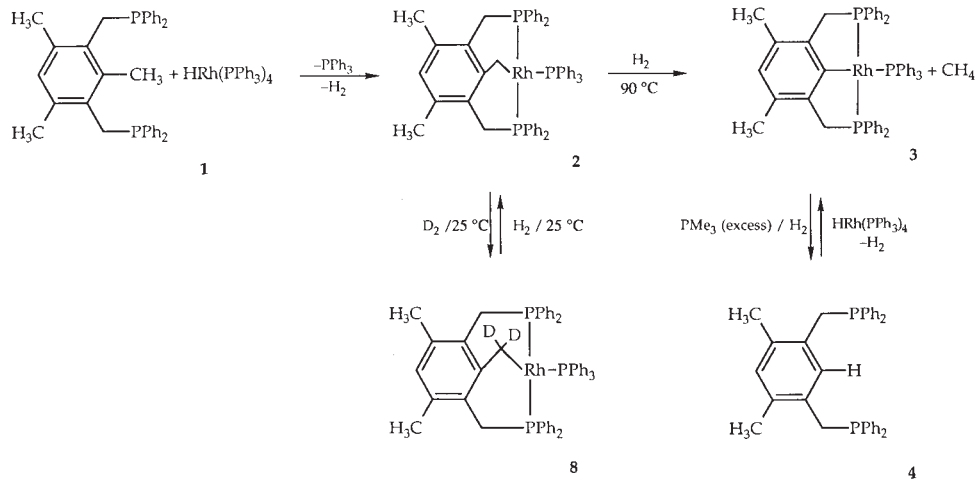

FIG. 2 Experiments demonstrating competitive C–H and C–C activation, resulting in selective C–C hydrogenolysis. (Ph is a phenyl (C_6H_5) group, Me is a methyl (CH_3) group.)